GRC Transactions, Vol. 47, 2023

Energy Storage in Deep Hydraulic Fractures: Mathematical Model and Field Validation

Douglas Simpkins, Mauricio A. Rivas, Mike Eros and Lev Ring

Sage Geosystems

Keywords

Mechanical energy storage, field test, huff and puff, managed pressure power, multiscale fracture propagation, simulator, wellbore friction

ABSTRACT

There is growing interest in developing technology to store energy in deep hydraulic fractures, as this has the potential to offer numerous benefits over other forms of energy storage. One key advantage is that large amounts of energy can be effectively stored in a relatively small footprint, which is particularly important in areas where land is at a premium. Additionally, subsurface energy storage can be more reliable and predictable than other forms of energy storage, as it is less subject to weather and other external factors that can affect the performance of above-ground systems. There is also potential for subsurface energy storage to be used in conjunction with hot dry rock (HDR) geothermal energy, which could further increase the overall round trip efficiency and value of the system.

To test the proposed storage concept, a deep plugged and abandoned well in South Texas was re-entered, re-completed and a vertical downward fracture was created. Multiple test cycles were performed that injected fluid into this created fracture and then produced it to the surface under pressure. Power generation was simulated by flowing through the controllable choke and measuring pressure drop as well as flow rate and temperature across the choke. The tests show that deep fractures can be used to store and recover energy.

A mathematical model has been developed for simulating, evaluating, and analyzing subsurface mechanical energy storage systems. Governing physics underlying the simulator include: (1) the near-tip behavior of propagating fractures governed by competing dissipative processes and fluid balances; (2) interactions with the reservoir; (3) non-isothermal wellbore hydraulics; and (4) surface equipment behavior.

The developed mathematical model was calibrated and validated against real-time data obtained during the five weeks of tests with varying duration of injection/production cycles and different fluid volumes and pump/flowback rates.

One of the main benefits of this novel energy storage technology is that it is scalable now as it relies on current, commercially available equipment that can be adapted to a broad range of subsurface conditions. Any intermittent renewable (such as solar and wind farms) can be easily paired with this technology to store mechanical energy to be delivered during times when these intermittent generators are not producing, making them 24/7 baseload. Although the best utilization for this energy storage is to pair it with wind and solar, it can be paired with any energy generation system (nuclear, gas, etc.) Modeling and simulation are, thus, imperative for optimizing system configurations before engineering commercial operations.

1. Introduction

Decline in costs of intermittent renewables, such as solar and wind power generation, has led to an increased deployment of these energy resources, which in turn has augmented the need for energy storage capacity. Currently pumped hydro energy storage (PHES) accounts for 96% of global storage power capacity and is cheap for large-scale energy storage, while batteries are rising competitors for short-term storage. See Figure 1 taken from the IRENA (2017) report on projections of storage capacity; see Blakers et al. (2021) for a review on the above topics that also discusses off-river pumped hydro systems that reduce environmental costs as PHES is typically limited to mountainous areas.

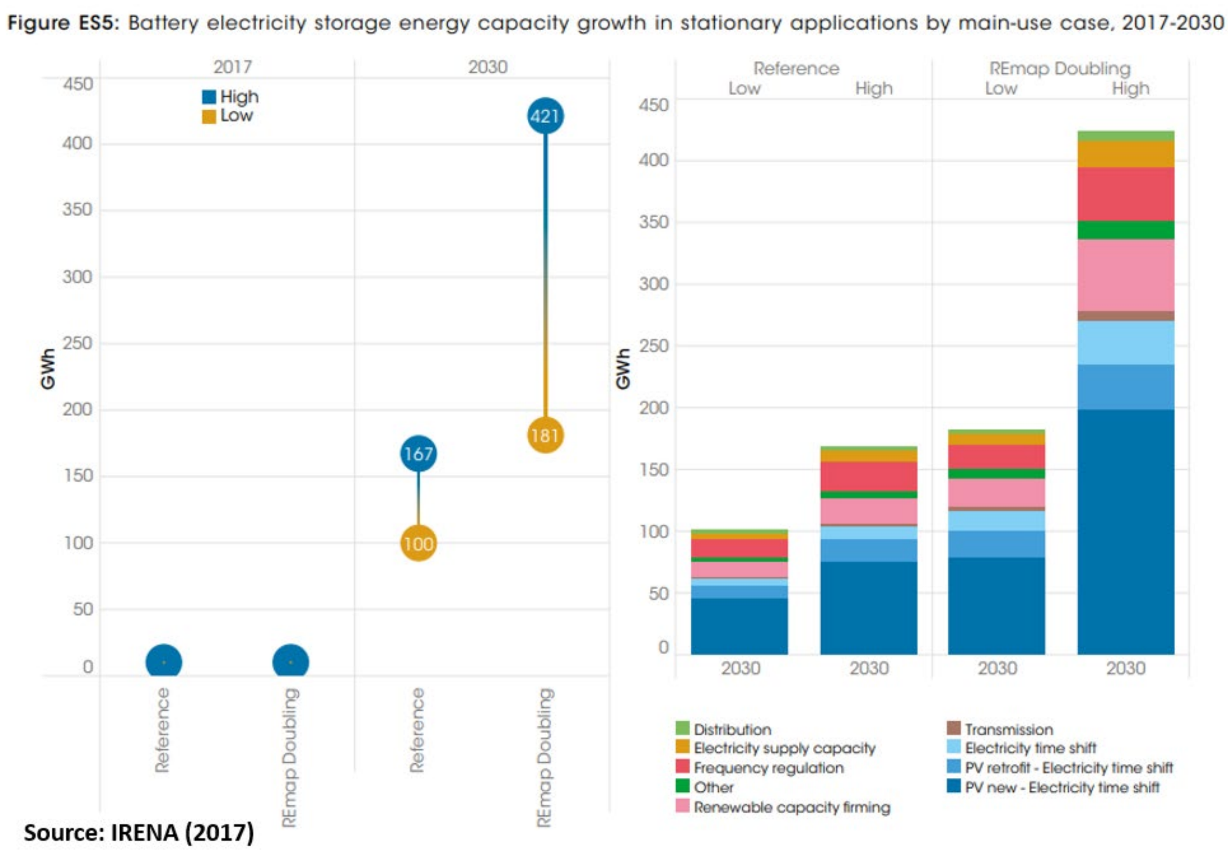

Figure 1: Projections are large for battery energy storage capacity. In the REmap Doubling case, the share of renewable energy (RE) in the global energy system is doubled from 2014 levels, and projections for this case are compared to the reference projections.

Mechanical energy storage, in the form of pressurizing deep hydraulic fractures as described in Section 2, is an emergent alternative to pumped-hydro and battery energy storage for the following reasons. First, mechanical energy storage is not geographically limited to mountainous or near-river locations as it can be sited essentially anywhere. Secondly, the pressurized system can produce small (1 MW) to large (1 GW) electric power output, whereas PHES usually needs to be sized between 100 MW to 3 GW to be economical. Next, mechanical storage has a small surface footprint, which is about four to ten times smaller than PHES, but the energy density (due to fracturing at great depth) is ten times greater than PHES. Moreover, obtaining permits for constructing mechanical energy storage facilities is a process that takes much shorter times (a few weeks in Texas) in contrast to the decades that hinder the completion of PHES projects. Furthermore, mechanical energy storage at scale has a lower Capital Expenditure / Levelized Cost of Storage (CAPEX/LCOS) than PHES; compare $2 million per MW to $2.64 million per MW, respectively; see NREL (2023). Lastly, an individual mechanical energy storage system can dispatch power at varying rates by changing flow rates, which is a challenge for battery storage solutions.

A field test in South Texas, see Figure 2, has successfully demonstrated *managed pressure power,* defined here as power obtained from an adaptive subsurface pumped storage process that precisely controls the pressure in the wellbore/fracture system; the objective is to ascertain the pressure environment of the fracture system downhole and to manage the system pressure profile accordingly to produce the desired power at surface. The South Texas demonstration thus exhibited the viability of the mechanical energy storage concept as an alternative to (at surface) pumped-hydro and battery energy storage. During the field testing the following were displayed: large amounts of energy were stored mechanically by pumping fluid into a single deep vertical hydraulic fracture and then the energy was efficiently extracted; the site occupied a small area at surface; and development of the site relied on readily available oil and gas technology. Moreover, according to the seismic array installed by the University of Texas at Austin Bureau of Economic Geology prior to operations with continuous public recording as part of the TexNet observation network, there was no induced seismicity detected during fracturing and subsequent pumping operations (http://www.beg.utexas.edu/texnet/catalog/ ; TexNet-CISR (2021-2023)).

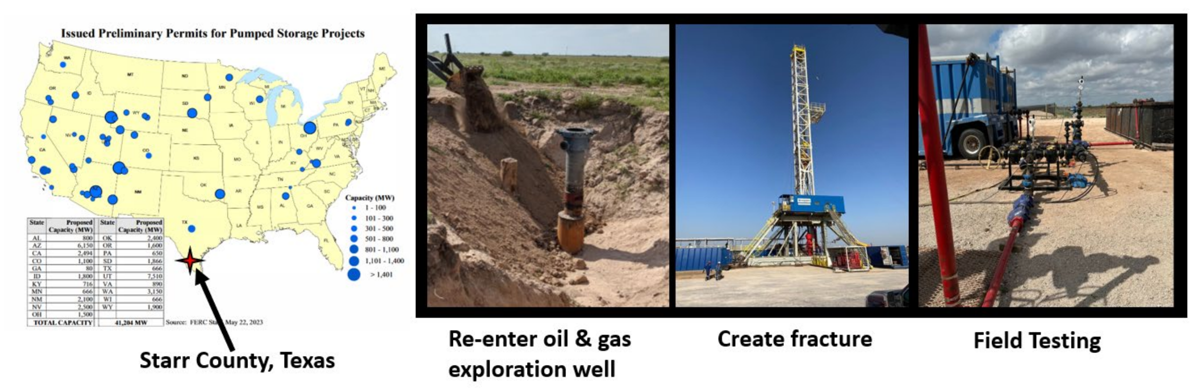

Figure 2: Location and pictorial timeline for the Mechanical Energy Storage field test at Starr County, Texas. The map shows pumped storage projects with preliminary permits from the Federal Energy Regulatory Commission (FERC) as published on May 22, 2023.

A mathematical model has been developed to simulate and analyze the mechanical energy storage system described in Section 2. The model captures: the deformation and multi-scale nature of fracture propagation; wellbore friction; pressure response due to injection pumping, shut-in, and production; and power conversion models. Section 4 presents the associated governing equations.

In this paper, the simulator is used to digitally replicate the South Texas field test results. Benchmarking shows evidence that the developed model predicts the behavior and outcomes of the managed pressure power operations that were performed in the mechanical energy storage demonstration in South Texas. Section 3 presents some of the cycles of energy storage conducted at the South Texas site that illustrate the attainment of managed pressure power, and these cycles are used for benchmarking in Section 5.

2. Mechanical Energy Storage System

The framework of an energy-storage system comprising a single well and a single hydraulic fracture is presented in Figure 3. To exemplify the utility of the system, the injection/production timings are chosen as if the system were connected to solar power and operating to help flatten the so-called *duck curve* associated with the penetration of solar power generation; see Denholm et al. (2008). The system, however, can be connected to other intermittent renewables such as wind power, or to the utility grid to move energy from time periods when demand is low to those time periods when demand peaks.

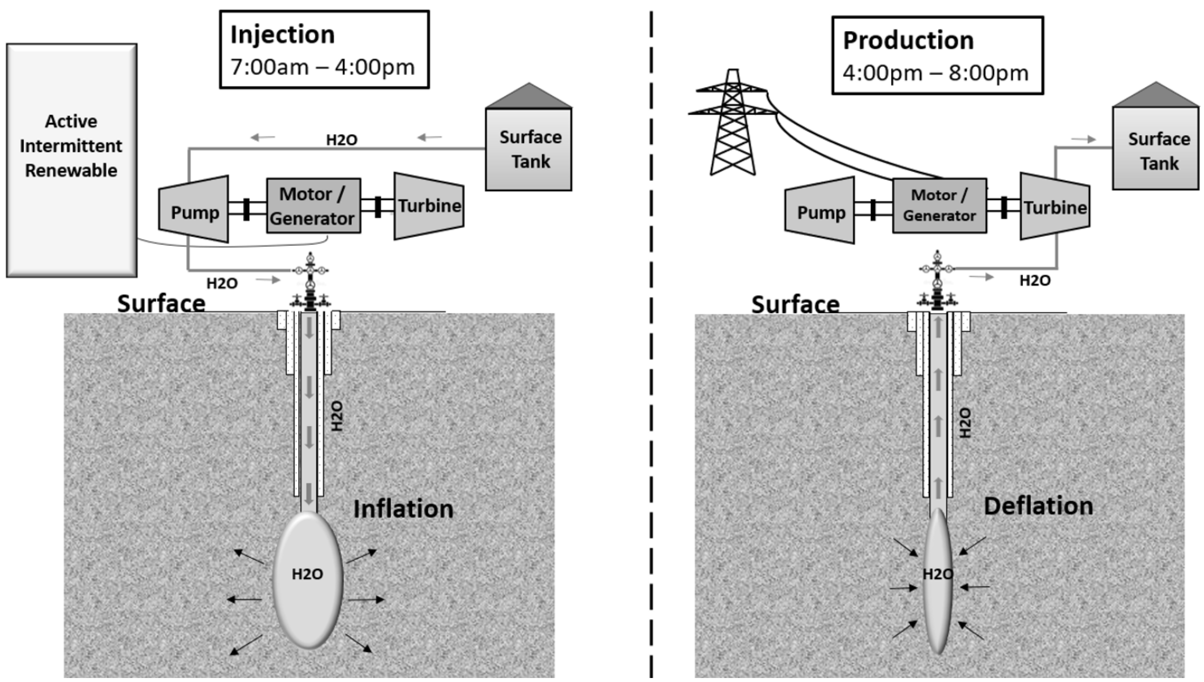

Figure 3: Framework of a single-well/single-fracture mechanical energy storage system. Left shows system during off-peak hours (on a sunny day) and right shows system during peak-hours (after work/school).

This system behaves as follows: during off-peak hours (left of Figure 3), the system is pressurized with an electrically driven pump that inflates the fracture with fluid and stores mechanical energy through the elastic compression of rock in the deep low-permeability rock reservoir region. The system is, and can be maintained, shut-in when the appropriate pressures are reached. Then the system is partially vented during the subsequent period of peak power demand (right of Figure 3), returning the previously stored mechanical energy. During the production phase of the cycle, this recovered energy is then converted to electrical energy via a hydroturbine. Similar inflation-deflation processes are sometimes called huff-and-puff cycles in the oil and gas industry.

Creating a multi-well system based on this concept enables the engineering and development of a high-capacity mechanical energy storage system. Figure 4 below is a rendering of such a system with 20-30 MW power capacity where ten wells are connected at surface and are serviced by several injection pumps, turbines, and an adjacent surface water pond. Distance is scaled to aid the visual, but it is worth noting that the surface footprint is still relatively small; a multiple-well system with 10 to 20 wells can be constructed from a pad at surface that occupies less than 5 acres (excluding water storage).

Construction of such multi-well systems is currently possible by implementation of multi-well pad drilling techniques that have been used in the oil and gas industry for the past 15-20 years for unconventional shale development. The short distance at surface between wells enables movement of the entire drill rig from well to well without it being disassembled. This 'walking drilling rig', as it is usually called, leads to: (1) having a smaller surface footprint; (2) significant improvements in efficiencies and thus reductions in costs; and (3) supply chain advantages.

Figure 4: Rendering of a surface layout of a high-capacity mechanical energy storage system.

The rendered design shows, from the pedestrian's point of view, ten wellheads to the left, five injection pumps to the right, and five hydro turbines further ahead placed on top of a tank to capture the discharge water. All these components sit next to a water-storage facility (pond).

3. Experimental Data from Field Testing Mechanical Energy Storage

3.1 Test Site Location and Wellbore Description

Siting, construction and field test operations (see Figure 2 photos) took place in Starr County located in South Texas at the site (coordinates 26°34′34.8040", 98°34′01.6664") that is about 30 miles northeast from Rio Grande City, TX, and about 45 miles northwest from the city McAllen, TX. The abandoned gas exploratory well at this location is named JFB Heard Estate 1. Figure 5 pinpoints the test site and gives a satellite view of the well that is also seen in Figure 2.

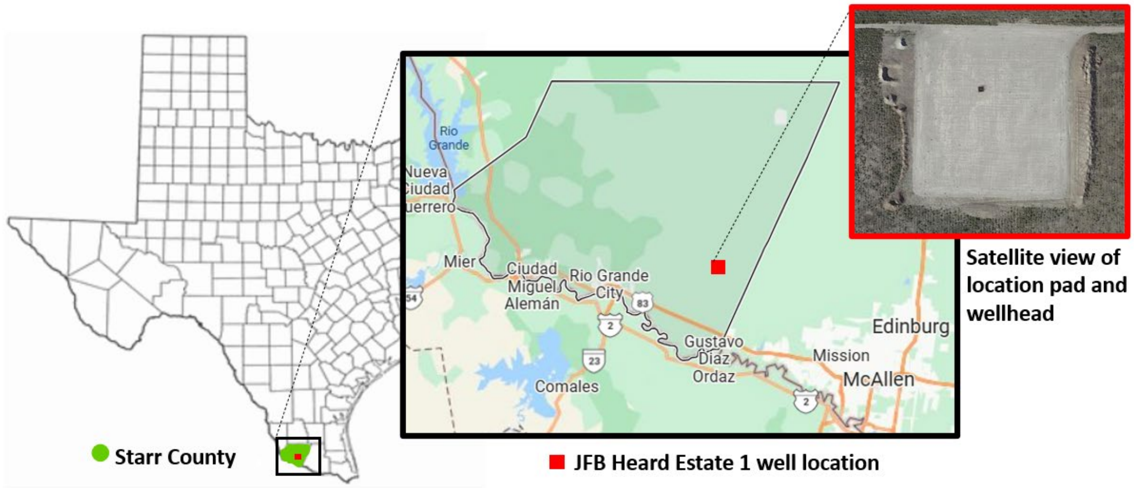

Figure 5: Telescoping view of the well (appearing as a black dot in the right image) used for the Mechanical Energy Storage field demonstrations.

The well JFB Heard Estate 1 was drilled as a gas exploration well targeting Paleogene reservoirs, reaching a total true vertical depth of about 19,000' with casing run to a depth of about 11,500'. The geologic sections encountered at this site comprise the Vicksburg, Yegua, Cook Mountain, Weches, Queen City, Reklaw, and Wilcox formations. The lower Vicksburg section consists of transitional facies down to about 9,300' MD; competent mudstones and siltstones dominate the section below 9,500' down to 11,500' MD, i.e., down to the bottom of the cased interval.

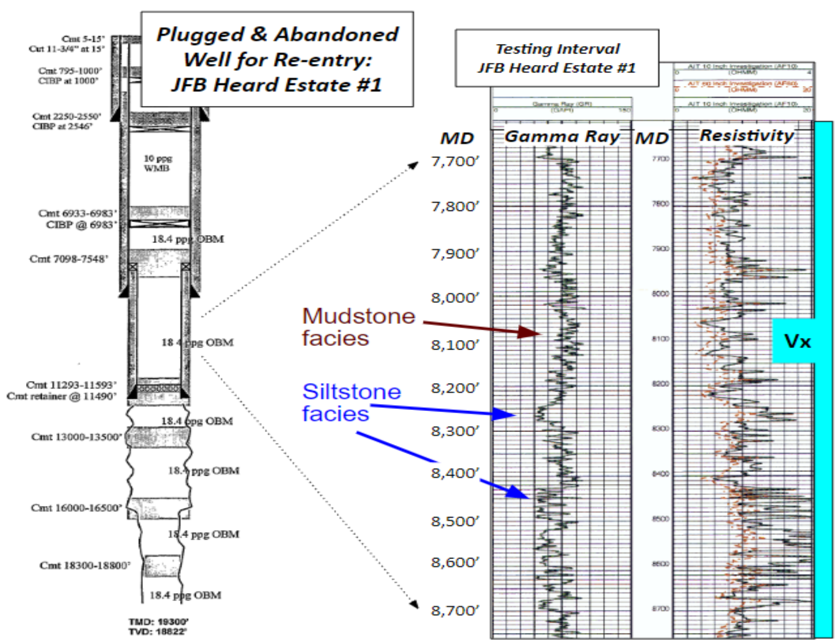

Figure 6: Subsurface data of the re-entered P&A well (seen in Figure 2 and 5) at the Starr County test site in South Texas showing well completion and gamma ray/resistivity logs for the testing interval.

Gamma ray and resistivity logs were employed to re-survey and confirm depths of the various formations. For demonstrating the pumped hydraulic fracture energy storage system, formations with low estimated permeability were targeted. Higher permeability formations and natural faults/fractures are typically avoided to minimize water/working-fluid leak-off and reduce induced seismicity risk. The original completion of the abandoned well and log plots in Figure 6 focus on the targeted zone for pumped storage. It was decided not to re-enter the deeper non-cased interval in the JFB Heard Estate 1 well, focusing on the Vicksburg formation mudstone/siltstones between 8,000' and 11,500'. The 9-5/8" drilling liner was tied-back to surface, providing a uniform inner diameter of the wellbore from surface to TD.

3.2 Engineered Deep Hydraulic Vertical Fracture

Between November 2021 to April 2022, a vertical fracture was created using a high-density fracturing fluid and a connection was made, confirmed through subsequent pumping operations, between perforations 3,200-feet apart in the well (~7,900'-11,100' MD). For this stimulation operation, small rig pumps were used (instead of a traditional frac fleet that have much larger costs and footprint) given the lower required pressures and volumes required for the gravity-driven technique applied. In later experimental preparation, deeper perforations were isolated and new perforations were made in a specific testing interval between ~7920' and ~8425' MD, giving access to a section of the previously gravity-fractured Vicksburg formation. It should be noted that with depth come higher energy densities as deeper fractures typically have higher closure pressures. Moreover, formations at deeper depths, in general, have lower porosities and permeabilities, as documented by Bebout et al. (1978) for this region of South Texas. In mechanical energy storage systems, fluid leak-off from the fracture is a source of potential losses and thus the lower the permeability, the lower the losses.

After initial field testing in 2021/2022, the JFB Heard 1 well was shut-in with plans to be re-entered at a later date for extended field testing of mechanical storage technology. Construction of a 30,000-barrel water storage facility at surface began at this time to enable the planned longer-duration huff-and-puff (or cyclic) operations; volumes of water were previously limited as steel tanks for water storage were used (see Figure 7 showing tanks and the facility for water storage). Continuous monitoring for induced seismicity was installed from October 2021, and it is reported that induced seismicity was not detected at the site during the stimulation or subsequent pumping operations (this data is available to the public online via TexNet, 2021-2023).

Figure 7: Steel tanks and the 30,000-barrel water storage facility built at the Starr County, Texas site.

3.3 Field Data on Managed Pressure Power

With the surface water storage facility in place, the single-well/single-frac system was re-entered in February 2023 and five weeks of testing commenced to demonstrate the mechanical energy storage concept. The test cycles produced *managed pressure power* in a way that demonstrated the energy storage system's potential for (1) electric load-following, i.e., the capability for a significant, and very rapid, increase in power output upon demand, and (2) long-duration energy storage as observed in the following sample cycles.

A huff-and-puff cycle that produced a long-duration constant power output was conducted on March 8, 2023 and is shown in Figure 8. Here an 8-bpm injection that lasted 8 hours (minus a 30 min gap) increased the subsurface volume by 3,601 barrels of water and consequently increased the pressure at the choke to 3,441 psi. The system was shut-in for 9 minutes, and then the added volume of water was produced to the surface at a rate that slowly increased from about 4 bpm to just above 6 bpm. This flowback produced an essentially constant 200 kW power output for the duration of 15 hours and 33 minutes. Power output for all cycles is calculated using equation (9) given in Subsection 4.2 that takes into account the efficiency of the hydroturbine.

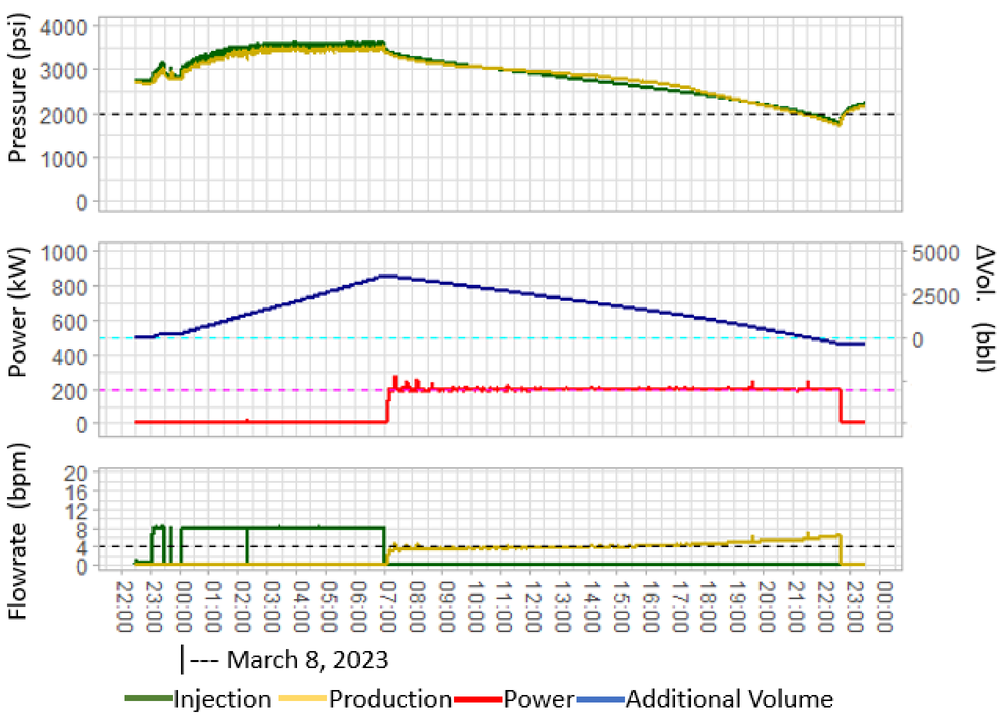

Figure 8: Huff-and-puff cycle producing constant 200 kW power for 15.5 hours.

A huff-and-puff cycle that produced a higher constant power output was performed on February 25, 2023 and is shown in Figure 9. For this cycle, an 8-bpm injection that lasted 23 hours and 10 minutes increased the subsurface volume by 11,122 barrels of water and consequently increased the pressure at the choke to 3,756 psi. The system was shut-in for 54 minutes (there was a short 14-minute flowback in between), and then a fraction of the added volume of water was produced to the surface at a rate that slowly increased from about 6 bpm to 10 bpm. This flowback produced an essentially constant 450 kW power output for 5 hours and 52 minutes.

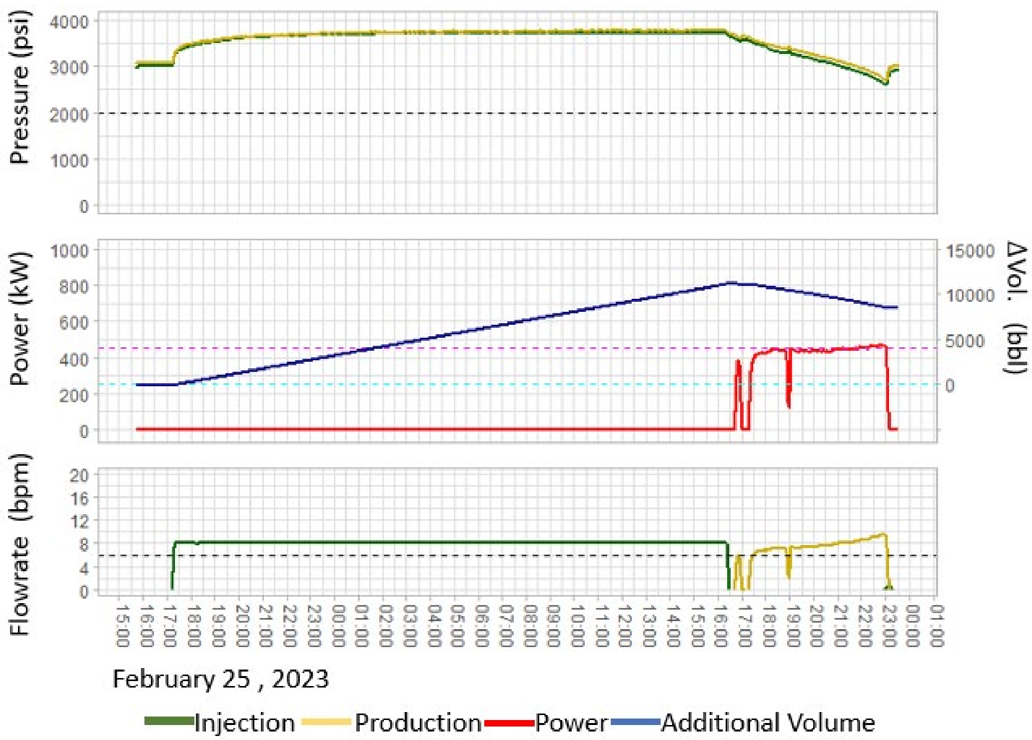

Figure 9: Huff-and-puff cycle producing constant 450 kW power for 5.8 hours.

The full amount of 11,122 barrels of water was not produced in this February 25 cycle in preparation for a subsequent long-production of power cycle on the following day. That cycle (not shown in this paper) delivered a near constant 200 kW of power during the corresponding 15-hour flowback after injecting another pad of volume of water; the power profile for that long-production cycle was slightly increasing whereas the power profile in Figure 8 is essentially constant.

Note that the pressure profile remained above 2,500 psi the February 25 cycle but dropped just below 2,000 psi in the March 8 cycle that produced to the surface the entire additional volume injected. In the following huff-and-puff cycles presented, the pressure profiles were controlled to be contained roughly in the 3,000-4,000-psi range during shut-in and inflation of the fracture. To prepare for a production event, the fracture was inflated until reaching the appropriate calculated volume and pressure required for the desired power output. Then production was active until pressure fell below 2000 psi at which time the system was shut-in.

In Figure 10 it is seen that by further increasing the production flowrates (compared to the flowrates in Figures 8 and 9), the higher constant power output of 500 kW was achieved for 2 hours and 6 minutes in the huff-and-puff cycle conducted on March 20, 2023. In this cycle, an 8-bpm injection that lasted 2 hours and 46 minutes (minus a 7 min gap) increased the subsurface volume by 1,269 barrels of water and consequently increased the pressure at surface to 3,450 psi. The system was shut-in for 3 minutes, and then the added volume of water was produced to the surface at a rate that gradually increased from 8 bpm to 12 bpm.

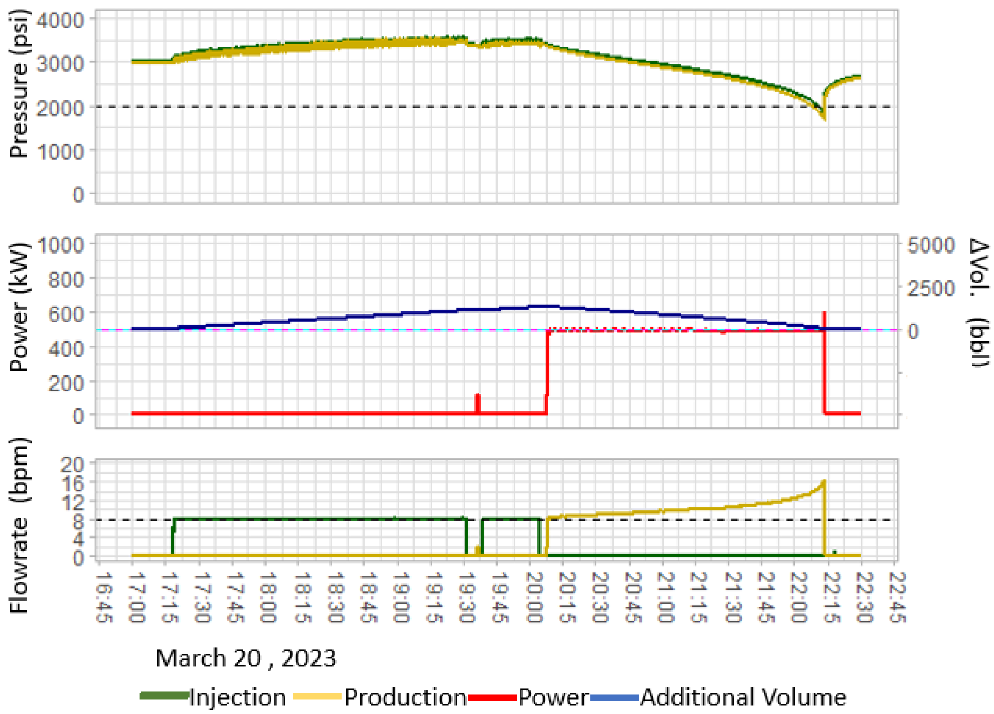

Figure 10: Huff-and-puff cycle producing 500 kW power for 2 hours.

Increasing the flowrates even higher led to a cycle with a constant power output of 650 kW; this was conducted on March 21, 2023 and is shown in Figure 11. The fracture inflation for this case was at an 8-bpm rate that lasted 3 hours and 18 minutes and increased the subsurface volume by 1,582 barrels of water and consequently increased the pressure to 3,488 psi. The system was shut-in for 3 minutes, and then the fracture was partially vented at a rate that gradually increased from 10 bpm to 20 bpm to return (most of) the added volume of water. This flowback produced an essentially constant 650 kW power output for 1 hour and 9 minutes (with a 3-minute gap). Note that this huff-and-puff cycle was performed immediately following the test cycle recorded in Figure 10 that produced 500 kW of power for 2 hours.

The March 21 cycle should be compared to the earlier cycle of March 15, 2023 shown in Figure 12, where the same extreme values for the production flowrate profile led to a cycle with the same constant power output of 650 kW but for almost twice the duration of 2 hours and 7 minutes. The fracture inflation for this case was also at an 8-bpm rate but lasted 4 hours and 12 minutes and thus increased the subsurface volume by the higher amount 2,001 barrels of water. However, the pressure at the choke increased to 3,440 psi, which is close to that of the March 21 cycle. The system was shut-in for 5 minutes, and then the added volume of water was produced to the surface at a flowrate that gradually increased (at a slower pace than that of the March 21 production) from 10 bpm to 20 bpm to return the added volume of water.

This brief comparison of cycles with equal power output but different production duration indicates that the attainment of managed pressure power is highly sensitive, among other variables such as fracture base fluid volume (see Section 4), to the pressure profile that is controlled by the flowrate profile. The sensitivity is further noticeable by contrasting with the pressure profiles in the other cycles recorded in this paper.

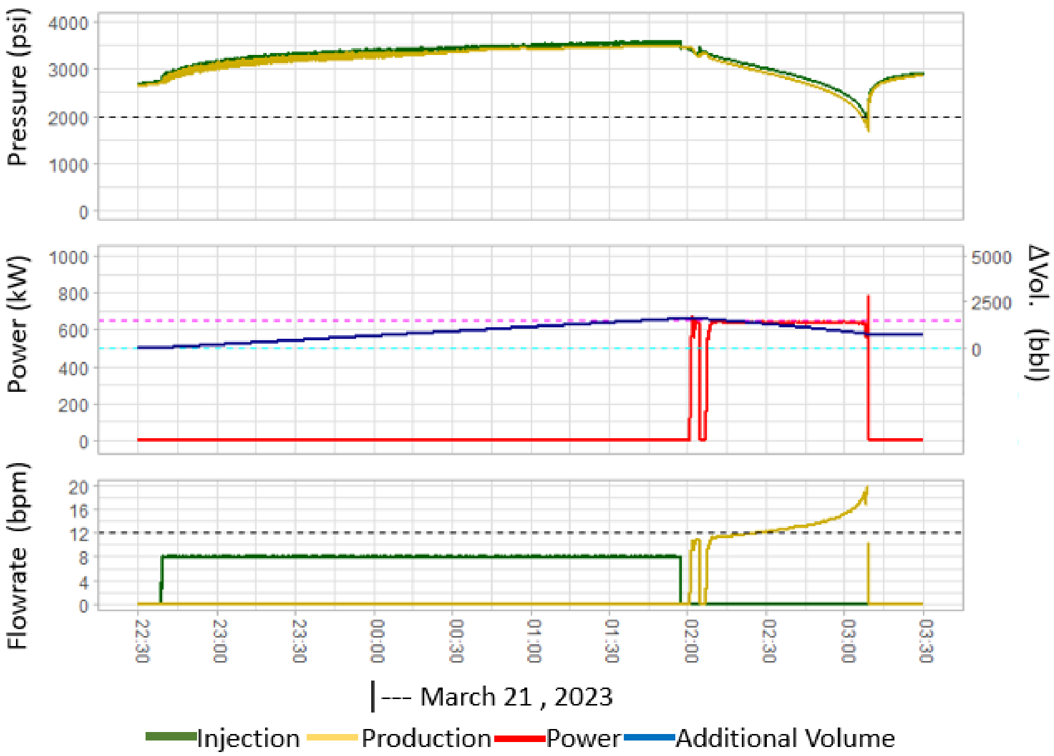

Figure 11: Huff-and-puff cycle producing 650 kW power for 1 hour.

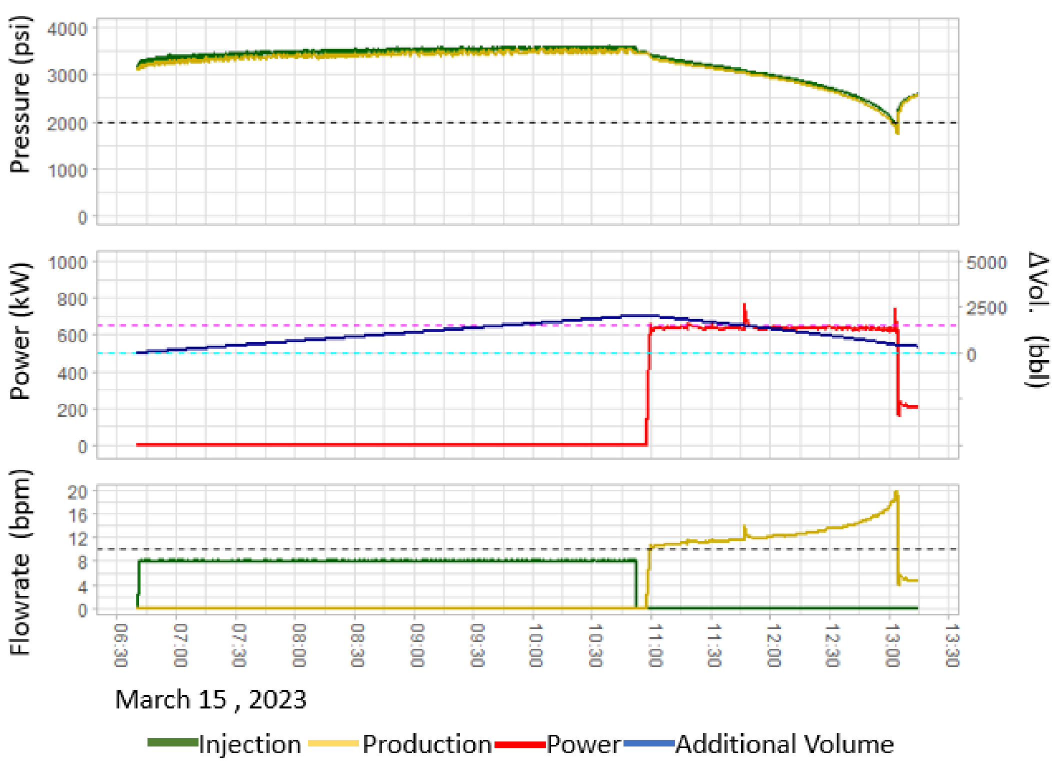

Figure 12: Huff-and-puff cycle producing 650 kW power for 2 hours.

In the huff-and-puff operations recorded above, the objective was to obtain a constant power production and this goal was achieved by generating the appropriate pressure profile from a suitable increasing production flowrate profile. Now it is observed in Figure 13 that by setting the production flowrate to a higher but constant rate, a dispatch of high power is obtained. This cycle was conducted on March 10, 2023 and had an 8-bpm injection that lasted 2 hours and 19 minutes that increased the subsurface volume by 1,102 barrels of water which in turn increased the pressure to 3,431 psi. The system was shut-in for 6 minutes, and then the added volume of water was produced to the surface at a near constant rate of 18 bpm. An average of 742 kW of power was produced during this 44-minute flowback, with a peak power of near 1 MW (there are 1067 kW values recorded).

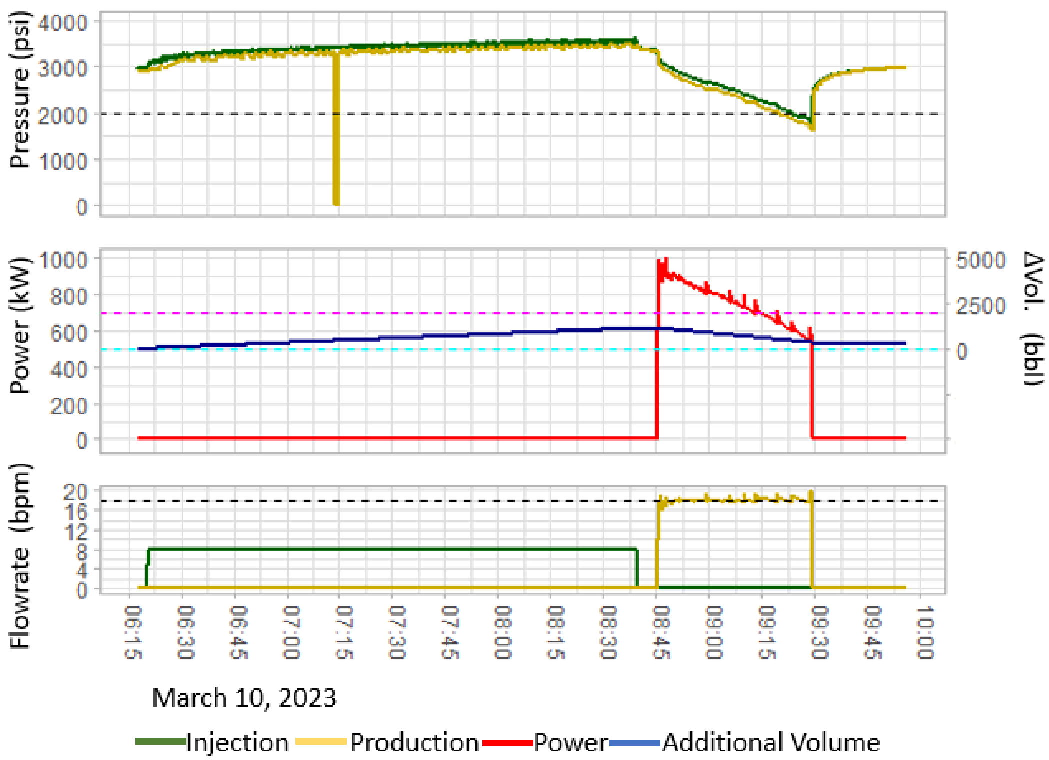

Figure 13: Huff-and-puff cycle with 1 MW peak power from a 44-minute flowback.

In summary, the appropriate production flowrate profiles allowed controlling of the pressure profiles that led to constant-rate or peak power outputs. The field tests show that power with varying rates is highly dispatchable from this individual single-well/single-frac storage system, in contrast to the capabilities of an individual battery storage system. It is to be noted that the maximum power generated was constrained by surface facilities, and that the spin-up time to maximum power was less than 30 seconds, satisfying the criteria for most ancillary services to the grid.

In addition to the above, *long-duration energy storage* was also exhibited in the South Texas field tests, as observed in the huff-and-puff cycle recorded in Figure 14. On the morning of March 21, a volume of 1,119 barrels of water was injected between 5:39 am and 7:59 am. At this time the subsurface system was shut-in for 3 hours and 41 minutes before four 10-minute (approximately) productions occurred that reduced the additional volume to 975 barrels. The system was maintained shut-in until the next day. On the morning of March 22, an additional 355 barrels of water was injected in a time window of 45 minutes that increased the pressure at surface to 3,270 psi. Then the system was shut-in again, this time for 3 hours and 52 minutes. Power was then produced at about 350 kW for 3 hours and 6 minutes. This finished a complete huff-and-puff cycle (i.e., the entire additional injected fluid was produced) as seen by the blue curve, but the system was maintained on production mode at 200 kW for an additional 3 hours and 6 minutes afterwards.

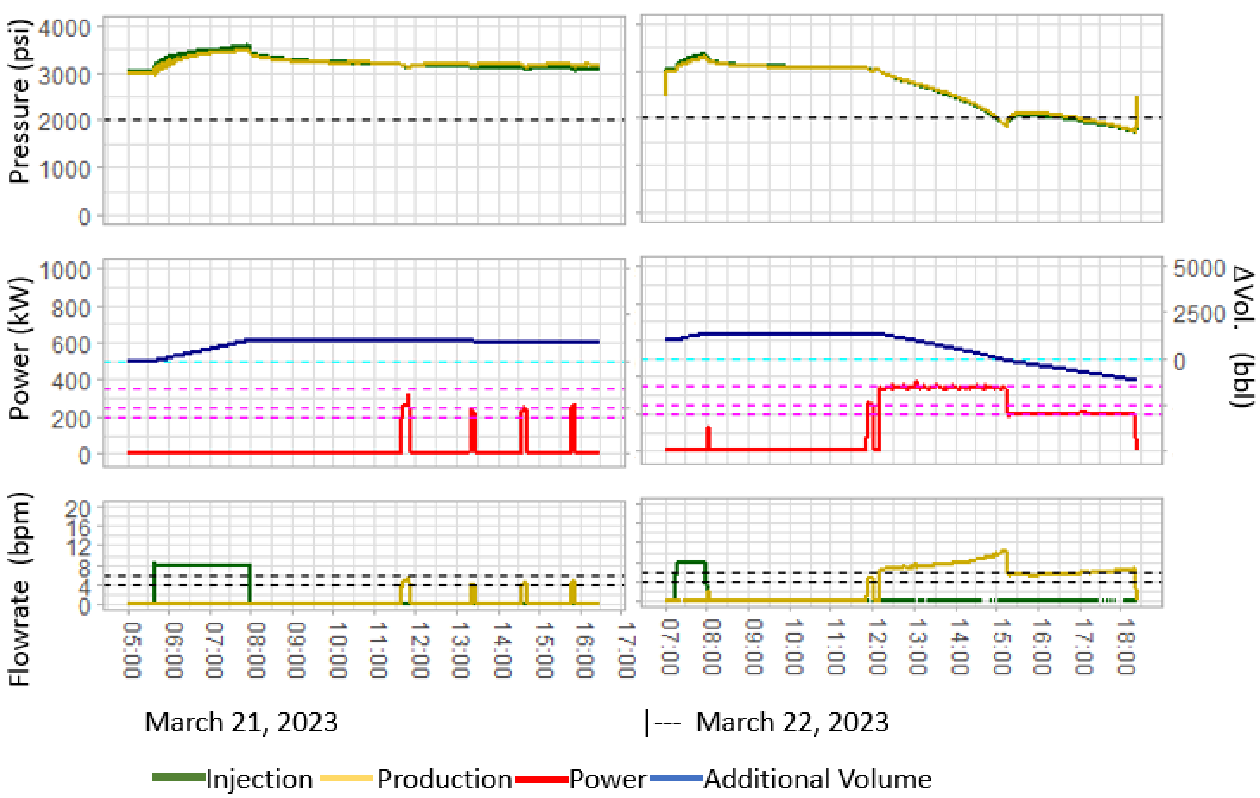

Figure 14: Long-duration energy storage (23 hours, then 4 hours) in a huff-and-puff cycle producing 350 kW power for 3 hours, with an extended output of 200 kW power for 3 hours.

Besides long-duration energy storage, this inflation-deflation cycle also demonstrates the agility of the energy storage system to switch power production levels and that the system can run past the complete huff-and-puff cycle (provided the pressures and volumes are precisely calculated).

We end this section by mentioning two different groups that have field tested the subsurface pumped energy storage concept. Schmidt et al. (2023) experimented also with single wells, but with horizontal fractures at shallow depths. Brown and DuTeau (1995) provided experimental and numerical results on load-following using the complex multi-frac system intersected with two wells at the Fenton Hill, New Mexico HDR site. The South Texas site, on the other hand, used a one-well/one-frac storage system that leveraged the high energy capacity that fractures at great depth provide to demonstrate both managed pressure power and long-duration energy storage.

4. Governing Equations

The behavior of the single-well/single-fracture system used for mechanical energy storage, as in Figure 3, is simulated with the following assumptions. A fracture containing water is embedded in an isotropic normally faulted low permeable mudstone that is characterized by shear-strain modulus $E' = \frac{E}{1-\nu^2}$, where E is Young's modulus and ν is Poisson's ratio; the fracture is assumed to have been previously installed in the formation. The minimum stress field σ_0 is linked directly to the fracture gradient. The fracture is connected to a single wellbore defined by a uniform casing with inner diameter ID and length L, and the fracture-well system maintains a varying volume of fluid by holding backpressure at the surface. During injection, the well is connected to a set of pumps, and during production the well is connected to a hydro-turbine, connected to a generator, followed by a choke. A surface pit holds any volume of water used for injection or production. Leak-off from the fracture to the reservoir is assumed to be negligible since the zone of interest is comprised of mudstone as mentioned in Section 3.1 and 3.2. Temperature and pressure effects on thermophysical properties are neglected.

Incompressible water is used as the primary fluid for injection and production. To prepare for a huff-and-puff operation, the fracture/wellbore system is assumed to contain a given volume of water called the *base fluid volume* and denoted by $V_{\mathrm{B,fl}}$. Then a given volume of fluid $V_{\mathrm{op,fl}}$, called the *operating fluid volume*, is injected into the well-frac system and then the total volume $V'_{\mathrm{fl}} = V_{\mathrm{B,fl}} + V_{\mathrm{op,fl}}$ is called the *prime fluid volume*.

The model components comprising elastic deformation, fracture fluid flow and part of the boundary and propagating conditions, are taken from Zia and Lecampion (2022) but tailored to model mechanical energy storage. Whereas equations concerning the behavior of wellbores, pumps, turbines, chokes and their interconnections are similar to those of the American Petroleum Institute (API) equipment and operating standards. Moreover, the subsurface pumped-storage modeling is in some ways similar to that of Bunger et al. (2023).

4.1 Elastic Deformation and Fracture Fluid Flow

For a planar fracture, the area is denoted by $A(t)$, the fracture aperture is given by $w(x, y, t)$ and the mode I quasi-static balancing of momentum leads to the relation

$$T(x,y) - \sigma_0(x,y) = -\frac{E'}{8\pi}\int_{A(t)} \frac{w(x',y',t)}{((x'-x)^2 + (y'-y)^2)^{\frac{3}{2}}} dA(x',y') \quad (1)$$

where T, σ_0 are, respectively, the normal components of the applied traction and in-situ compressive stress. The fracture may close but is bounded below by a residual aperture w_a defined as the minimum between the opening encountered thus far and a value related to the intrinsic roughness of the fracture. Contact conditions are thus given by

$$(w(x,y) - w_a) \geq 0 \quad \text{and} \quad \big(T(x,y) - p(x,y)\big)\big(w(x,y) - w_a(x,y)\big) = 0 \quad (2)$$

where p is fluid pressure. Conservation of mass in the fracture yields, assuming no leak-off as the target zone is comprised of mudstone (see Section 3.1 and 3.2), the relation

$$\frac{\partial w}{\partial t} + c_{\mathrm{f}} w \frac{\partial p}{\partial t} + \nabla \cdot \boldsymbol{q} = \hat{Q}(t)\delta(x - x_0, y - y_0) \quad (3)$$

where $\hat{Q}(t) = \lim_{V\to 0} \frac{\dot{m}(t)}{\rho V}$ is a 'point-source' flowrate, linked to mass-flowrate $\dot{m}$ via density ρ, which is positive for injection and negative for production, and $\boldsymbol{q}$ is the fluid-flux within the fracture that is given by a Darcy-type expression, with an equivalent permeability $w^2/12$, known as the 'cubic-law' relation

$$\boldsymbol{q} = -\frac{w^3}{12\mu}(\nabla p - \rho \boldsymbol{g}) \tag{4}$$

that is derived from the relation for laminar fluid flow between parallel plates; here, μ is viscosity and $\boldsymbol{g}$ is the gravity vector. Turbulence effects have been neglected and flow is assumed to be maintained in the laminar regime during mechanical storage cycles.

4.2 Wellbore, Injection Pump, Hydro-turbine and Choke

The wellbore is a vertical casing of uniform inner diameter d_{C}, length L, and hydraulic diameter given by $H_{\mathrm{d}} = d_{\mathrm{C}}$. The three phases of the mechanical energy storage system are: injection, shut-in, and production.

4.2.1 Injection

During the injection phase of the storage system, the bottom-hole pressure in the wellbore is determined by:

$$P_{\mathrm{BH}}(t) = P_{\mathrm{pump}}(t) + \rho L\left(g - \frac{8fQ(t)^2}{\pi^2 H_{\mathrm{d}}^3}\right) \tag{5}$$

with acceleration due to gravity g and Fanning friction factor f given by the Colebrook-White relationship, which for the transitional/turbulent regime, $\mathrm{Re} > 2100$, reads as

$$\frac{1}{\sqrt{f}} = -4\log_{10}\left(\frac{\varepsilon}{3.7H_{\mathrm{d}}} + \frac{1.255}{\mathrm{Re}\sqrt{f}}\right) \tag{6}$$

and for the laminar regime, $\mathrm{Re} \leq 2100$, reads as

$$f = \frac{16}{\mathrm{Re}} \tag{7}$$

where $\mathrm{Re} = \frac{4\rho Q}{\pi^2 \mu H_{\mathrm{d}}}$ is the Reynold's number. The power required by the injection pump at surface is determined by

$$\dot{W}_{\mathrm{pump}}(t) = \frac{\Delta P_{\mathrm{pump}}(t)Q(t)}{\eta_{\mathrm{pump}}} \tag{8}$$

where η_{pump} is the overall efficiency of the pump assumed to be around 0.85. The pump suction pressure is assumed to be taken at atmospheric pressure.

The power generated by the hydroturbine at the surface is determined by

$$\dot{W}_{\mathrm{turb}}(t) = \Delta P_{\mathrm{turb}}(t)Q(t)\eta_{\mathrm{turb}} \tag{9}$$

where η_{turb} is the overall efficiency of the pump assumed to be around 0.9.

4.2.2 Shut-In

To keep the fracture filled with a given fluid volume V during the shut-in stage of the system, the bottom-hole pressure P_{BH} needs to be maintained. To accomplish this, the required backpressure is given by

$$P_{\mathrm{BP}} = P_{\mathrm{BH}} - \rho g L \tag{10}$$

4.2.3 Production

During production, a hydro-turbine is installed downstream of an adjustable choke which connects to the wellhead. The choke can be opened manually or automatically, dropping the back pressure to the well which allows the wellbore to flow. In this case, the flowrate is unknown and must be resolved. A pressure balance with the bottom of the well pressure in production is given by:

$$P_{\mathrm{BH}}(t) - \rho\left(\left(g + \frac{8fQ(t)^2}{\pi^2 H_{\mathrm{d}}^3}\right)L + h_{\mathrm{turbine}}(t)\right) - P_{\mathrm{choke}}(t) = 0 \tag{11}$$

and the turbine pressure drop is given in terms of the static available head h_{turbine}.

The pressure-loss across a choke in a non-choked flow is given by

$$P_{\mathrm{choke}}(t) = \frac{8\rho Q(t)^2}{\pi^2 C_{\mathrm{d}}^2 (\chi_{\mathrm{v}} d_{\mathrm{c}})^4} \tag{12}$$

where d_{c} is the upstream choke diameter and $\chi_{\mathrm{v}} = d_{\mathrm{choke}}/d_{\mathrm{c}}$ is the valve fraction open with d_{choke} the restricted diameter. In equation (12), the discharge coefficient C_d can be modeled by

$$C_{\mathrm{d}} = \chi_{\mathrm{v}} + \frac{0.3167}{\chi_{\mathrm{v}}^{0.6}} + 0.025(\log(\mathrm{Re_c}) - 4) \tag{13}$$

with the choke Reynolds number being defined by $\mathrm{Re_c} = \frac{4\rho Q}{\pi \mu d_{\mathrm{c}}}$.

4.3 Coupling Considerations and Boundary Conditions

For points (x, y) on the fracture front, at time t, of a propagating hydraulic fracture, we have

$$w(x,y,t) = 0, \qquad \boldsymbol{q}(x,y,t) \cdot \boldsymbol{n}(x,y,t) = 0 \tag{14}$$

Since the fracture is assumed to be propagating in a quasi-static equilibrium, the propagation condition becomes

$$\begin{cases} (K_{\mathrm{I}}(x,y,t) - K_{\mathrm{Ic}}(x,y) \le 0 \\ \left(K_{\mathrm{I}}(x,y,t) - K_{\mathrm{Ic}}(x,y)\right) \times V(x,y) = 0 \end{cases} \tag{15}$$

for points (x, y) on the fluid front. Here, $V(x, y)$ is the local fracture propagation velocity, $K_{\mathrm{I}}(x, y, t)$ is the stress intensity factor and $K_{\mathrm{Ic}}(x, y)$ is the fracture toughness of the material. However, see the work of Detournay et al. (2007) where they show theoretically that most hydraulic treatments are in the viscosity-dominated regime and where they also provide lab experiments confirming those results.

During a huff and puff operation the hydraulic fracture is assumed to not propagate (it is arrested), and this enforces the aperture at the fracture tip to be zero, so that the following hold, see Detournay and Peirce (2014):

$$w(x,y,t) = 0, \qquad \boldsymbol{q}(x,y,t) = 0 \tag{16}$$

The hydraulic fracture is coupled to the wellbore by either a pressure condition or a flowrate condition.

4.3.1 Injection

An injection $Q(t) > 0$ is prescribed for a period of time t_{inj}. The flowrate serves as volumetric flowrate point-source in equation (3) and pump pressure/work can be determined by equations (5) and (8). The bottom hole pressure is set equal to the fracture pressure $p(0,0,t)$.

4.3.2 Shut-in and Production

The system flowrate for a given time-step is determined by resolving equations (12) and (3) iteratively. The bottom hole pressure is again assumed equal to the fracture pressure $p(0,0,t)$. The turbine head $h_{\mathrm{turbine}}(t)$ is prescribed but limited by the maximum head available depending on the overall pressure balance.

4.3.3 Initial Conditions

A hydraulic fracture of volume V equal to the base fluid volume is given and is held at uniform initial pressure p_0. The pressure p_0 is determined by static conditions in the wellbore while shut-in pressure at the surface is found to maintain the volume V.

It was observed from huff-and-puff field data, that the hydraulic fracture during injections followed a PKN fracture behavior in the asymptotic case of a near zero leak-off. Thus, the pressure profile behaved as

$$p \sim t^{1/5} \tag{17}$$

See Valko and Economides (1995) and Economides and Nolte (2000) for a detailed description of the PKN model and its asymptotics with respect to fracture efficiency.

5. Results and Discussion

5.1 Validation with field data

The mathematical model described in Section 4 has been used to model the huff-and-puff operations from the South Texas field tests shown in Figures 8, 10, 11, and 13 of Subsection 3.3. Injection and production flowrates from the field data were taken as simulation input parameters, and the outputs resulting from the modeling are the backpressure profiles. Comparison of the modeled (black dashed lines) versus field data (red) backpressure profiles in the following figures indicates that there is good agreement between the digital replication and the actual South Texas mechanical energy storage operations. It is noted that the similar behavior of the pressures was found in Ricks et al. (2022) where the authors used ResFrac (a commercial reservoir simulation software) to simulate fracture behavior during injection and production cycles in an EGS reservoir (with one injector and two producer wells intersecting a multitude of vertical fractures). The modeling of the one-well/one-frac energy storage system in South Texas produced the following.

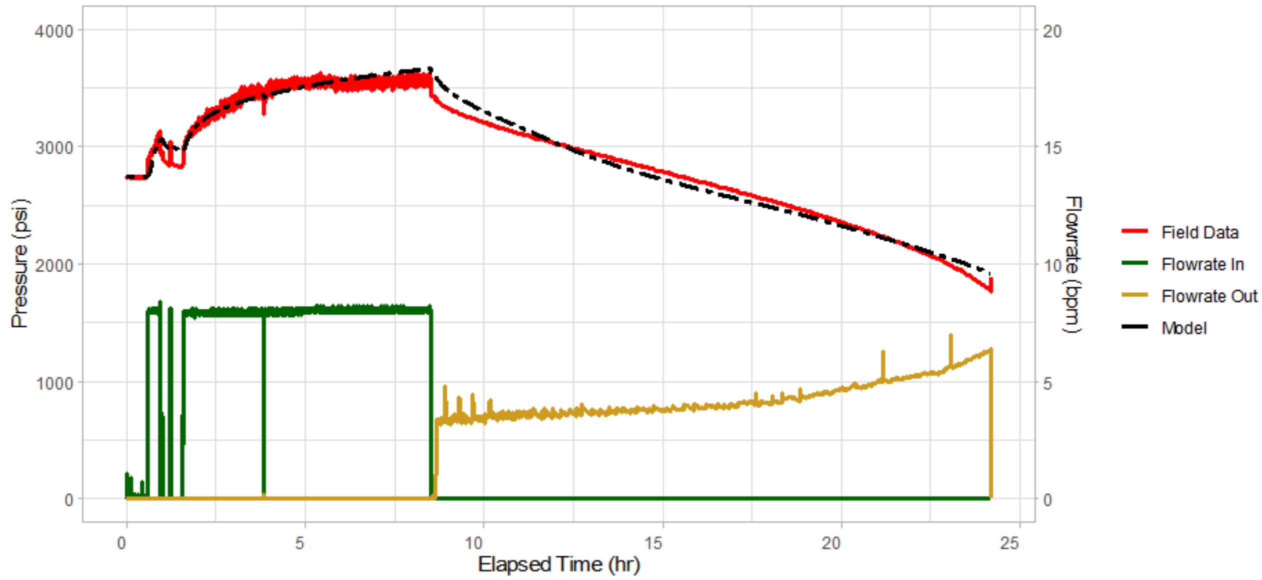

Figure 15: Comparison of pressure profiles from the mathematical model (black) and the operational data (red) for the huff-and-puff cycle with constant 200 kW power production lasting 15.5 hours.

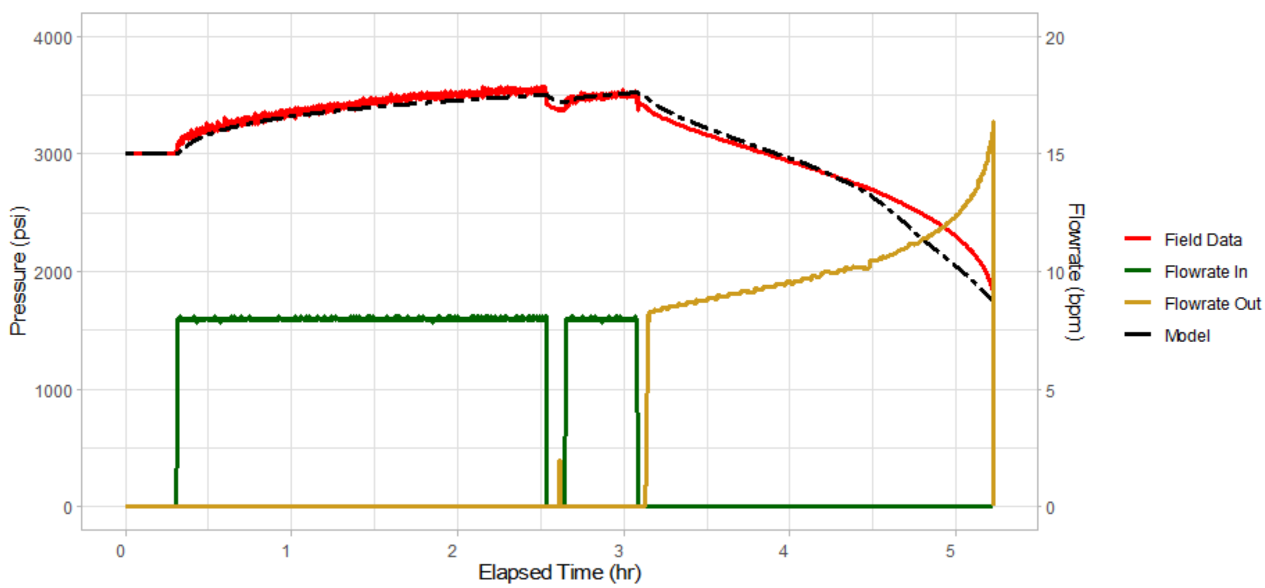

Figure 16: Comparison of pressure profiles from the mathematical model and field data from the cycle with constant 500 kW power production lasting 2 hours.

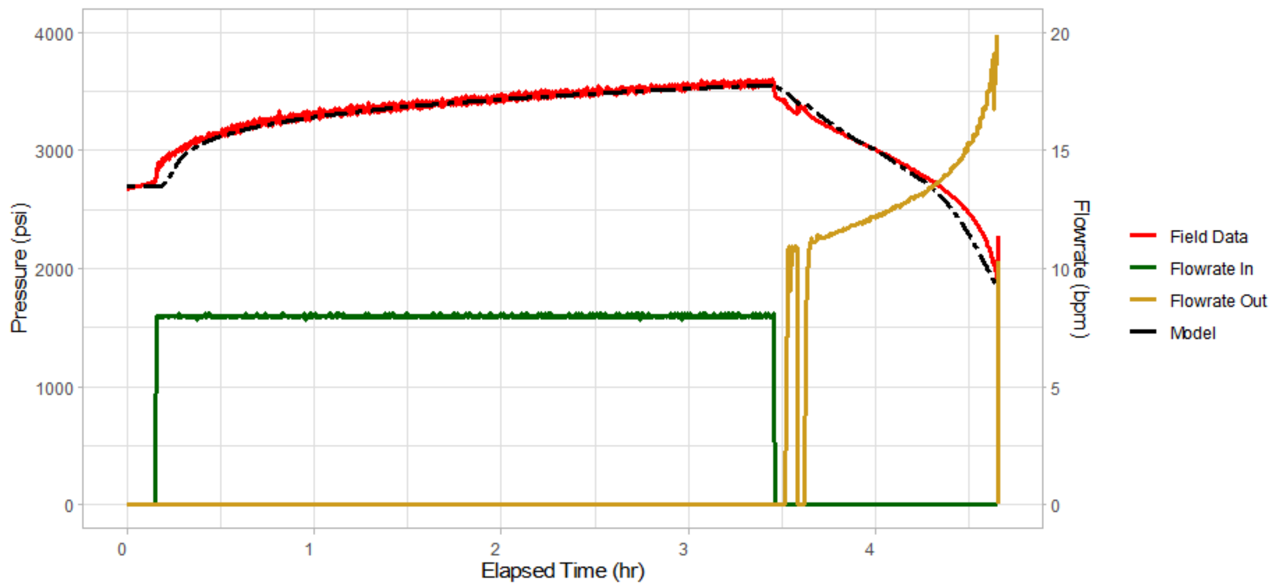

Figure 17: Comparison of numerical pressure profile with that of the actual profile from the field for the cycle producing constant 650 kW power for 1 hour.

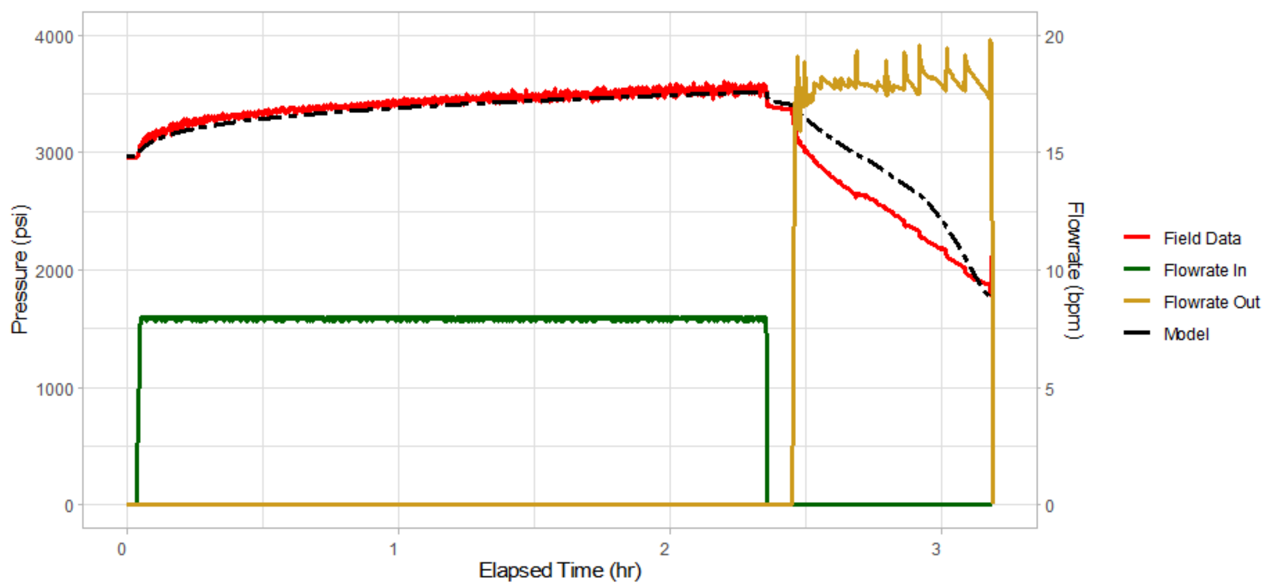

Figure 18: Comparison of numerical (black) and operational (red) pressure profiles for the huff-and-puff cycle with 1 MW peak power.

It is emphasized that the increasing profiles for production flow rates of the first three cycles were controlled to manage the pressure profiles that yielded corresponding constant-rate power outputs, whereas on the fourth cycle the production flowrate was near constant, but at a high value, and this sharply decreased the pressure profile which consequently produced a near linearly decreasing power output profile. These simulations (black dashed lines) show that the mathematical model is in good agreement with the field data and that the model may be used for predicting managed pressure power from the constructed energy storage system.

6. Summary and Conclusion

Testing of a pumped energy storage system, developed in South Texas in 2021, 2022, and 2023 of a system comprising a deep vertical hydraulic fracture connected to a single vertical well, demonstrated the ability to produce managed pressure power (as defined in the Introduction) with varying performance requirements. Long-duration power production was illustrated, for example, in the huff-and-puff cycle shown in Figure 8 where the constant 2 kW power production lasted 15.5 hours, and a 1 MW peaking power was evidenced in the cycle shown in Figure 13; also recorded in this paper were huff and puff cycles with 450 kW, 500 kW, 650 kW and 650 kW constant power productions lasting for 5.8 hours, 2 hours, 1 hour and 2 hours, respectively. These sample cycles also exhibited the capability for a significant and swift increase in power output upon energy requests/needs (i.e., dispatchable or load-following). Furthermore, long-duration energy storage and the agility to switch power output levels midway of a flowback were also displayed in the demonstration; these can be seen, for instance, in the inflation-deflation cycle documented in Figure 14. Therefore, the managed pressure power produced from this storage system has the potential, using the framework outlined in Section 2, to empower the renewable energy sector by enabling reliable and sustainable power generation.

As the demonstration relied on readily available equipment and procedures, this mechanical energy storage system provides an alternative to traditional pumped-hydro and battery storage with several key advantages. For instance, depth of the reservoir allows for a higher energy capacity, the technology has minimal geological and/or geographical limitations, and the single vertical well considerably reduces construction costs and/or permits for drilling new or repurposing existing wells.

A mathematical model has been developed to simulate the generation of managed pressure power from the energy storage system at the South Texas site. Good agreement was observed between the mathematical model and the huff-and-puff operations in this energy storage demonstration; the comparisons are seen in Figures 15 -18. This shows that the mathematical model may be used for optimizing future system configurations that are vital for planning and arranging commercial operations as well as the assessment of ongoing energy storage operations.

Acknowledgements

The authors gratefully thank the entire team at Sage Geosystems for the collaborative effort that permitted this multi process (engineering, geological, physical, mathematical and economic) machine to produce a successful energy storage demonstration. Special appreciation goes to Sage Geosystem's Summer 2023 Modeling and Simulation interns and apprentice, Victoria McGuire, Marina Ring, and Aileen Zebrowski, for assisting in the various tasks that helped shape and improve the writing of this paper.

REFERENCES

Bebout, D.G., Loucks, R.G., and Gregory, A.R., "Frio sandstone reservoirs in the deep subsurface along the Texas Gulf Coast – their potential for the production of geopressured geothermal energy." University of Texas at Austin, Bureau of Economic Geology report of Investigations, No. 91 (1978), 92 p.

Blakers, A., Stocks, M., Lu, B., Cheng, C., "A review of pumped hydro energy storage." *Progress in Energy*, 3 (2021) 022003.

Brown, D., DuTeau, R., "Using a hot dry rock geothermal reservoir for load following." *Proceedings, 20th Workshop on Geothermal Reservoir Engineering*, Stanford University, Stanford, CA (1995).

Bunger, A.P., Lau, H., Wright, S., Schmidt, H., "Mechanical model for geomechanical pumped storage in horizontal fluid-filled lenses." *International Journal for Numerical and Analytical Methods in Geomechanics*, Vol 47, Issue 8 (2023) pp. 1349-1372.

Denholm, R., Margolis, R., Milford, J., "Production cost modeling for high levels of photovoltaics penetration." NREL/TP-581-42305 (2008).

Detournay, E., Peirce, A., Bunger, A., "Viscosity-dominated hydraulic fractures." *Proceedings of the 1st Canada-US Rock Mechanics Symposium – Rock Mechanics Meeting Society's Challenges and Demands,* 2 (2007) 1649-1656.

Detournay, E., Peirce, A., "On the moving boundary conditions for a hydraulic fracture." *International Journal of Engineering Science,* 84 (2014) 147-155.

Economides, M.J., and Nolte, K.G., "Reservoir Stimulation." 3rd Ed., Wiley (2000).

IRENA (2017), Electricity Storage and Renewables: Costs and Markets to 2030, International Renewable Energy Agency, Abu Dhabi.

NREL (National Renewable Energy Laboratory). 2023. "2023 Annual Technology Baseline."

Ricks, W., Norbeck, J., Jenkins, J., "The value of in-reservoir energy storage for flexible dispatch of geothermal power," *Applied Energy*, 313 (2022) 118807.

Schmidt, H., Wright, S., Mauroner, C., Lau, H., Hill, B., Zhou, J., Bunger, A., "Geomechanical pumped storage in hydraulic fractures." SPE Hydraulic Fracturing Technology Conference and Exhibition. OnePetro (2023).

TexNet-CISR (2022-2023), Bureau of Economic Geology: TexNet Seismic Observatory and Center for Injection and Seismicity Research. https://www.beg.utexas.edu/texnet-cisr

Valko, P. and Economides, M.J., Hydraulic Fracture Mechanics. Wiley (1995).

Zia, H. and Lecampion, B., "PyFrac: a planar 3D hydraulic fracturing simulator." *Comp. Phys. Comm.,* 255:107368 (2022). http://doi.org/10.1016/j.cpc.2020.107368